



Selective hydrogenation of biomass-derived fatty acid methyl esters to fatty alcohols on RuSn–B/Al₂O₃ catalysts: analysis of the operating conditions and kinetics

María A. Sánchez¹ · María A. Vicerich¹ · Cristhian Fonseca Benítez¹ · Franco Nardi¹ · Francisco J. Passamonti¹ · Vanina A. Mazzieri¹ 

Received: 26 March 2024 / Accepted: 20 May 2024 / Published online: 27 May 2024
© Akadémiai Kiadó, Budapest, Hungary 2024

Abstract

Catalyst preparation, reaction process conditions and kinetics of the selective hydrogenation of fatty acid methyl esters (FAME) over a noble metal catalyst were studied. Two catalysts were prepared by impregnation of γ -Al₂O₃ with Ru (1% mass content) as active metal and Sn and B as modifiers (2% mass content), and with different Sn/Ru ratios of 2 and 4. FAME derived from biomass, an environment friendly raw material, was used for the preparation of fatty alcohols by selective hydrogenolysis of the ester group to an alcohol group. The results were analyzed with a simple kinetic model using lumped pseudocomponents. When comparing the two catalysts it was found that the most effective catalyst for producing oleyl alcohol was the one with a Sn/Ru ratio of 2, RuSn2–B. The maximum production of alcohols and alkanes was achieved with this catalyst at 290 °C. At 270 °C a lower production of alkanes was obtained but with a similar yield of alcohols. Both reaction conditions and catalyst composition were found to be important factors influencing alcohol production. Two types of active sites were identified on the studied catalysts: the unmodified Ru⁰ metal for dissociating hydrogen and the modified metal, (Ru⁰–(SnO_x)₂), for adsorbing the C=C carbons. RuSn2–B seemingly exhibited an appropriate balance of these sites. The kinetic model included the reactions of esters, hydrogen, alcohols and deoxygenated hydrocarbons. These were studied with lumped variables with no distinction of individual specific molecules. In spite of this, the model provided a very good fit of the experimental data indicating that the reaction is rather insensitive to secondary features like carbon chain length or group positions.

Keywords Biodiesel · Fatty alcohols · Selective hydrogenation · Kinetic model · RuSn–B/Al₂O₃

✉ Vanina A. Mazzieri
vmazzier@fiq.unl.edu.ar

¹ Instituto de Investigaciones en Catálisis y Petroquímica (UNL-CONICET), Colectora Ruta Nac. 168-Km 0–Paraje el Pozo, 3000 Santa Fe, Argentina

Introduction

The goal of the green oleochemical industry is to obtain products with properties resembling those of petrochemical products. The development of green oleochemical processes has recently been intensified due to the advantages environment friendliness of biodegradable and bioavailable precursors and products [1]. Fatty alcohols find applications in the manufacture of detergents, cosmetic emulsions (such as creams and lotions) to enhance consistency, and in industrial emulsions as co-surfactants or solubilizers [2]. Previous reports indicate that the global fatty alcohol market was valued at \$5.08 billion in 2019 and is projected to reach \$7.40 billion by 2027 [3]. Fatty alcohols are produced on an industrial scale by catalytic hydrogenation of fatty acids or their esters from vegetable oils at high pressure and temperature. Commercial processes for the synthesis of fatty alcohols typically use Cu–Cr-based catalysts under severe reaction conditions (250–350 °C and 10–20 MPa) [4, 5]. Recent studies have focused on replacing Cu–Cr-based catalysts with noble metal-supported catalysts [6, 7]. Supported RuSn–B catalysts have demonstrated activity and selectivity in producing fatty alcohols from esters or fatty acids [8–10]. In our previous research, we examined RuSn–B catalysts supported on Al₂O₃, SiO₂, and TiO₂ for the selective hydrogenation of methyl oleate and oleic acid to oleyl alcohol [11–16]. The supported catalysts demonstrated good activity, with a conversion rate between 80 and 90%, resulting in a yield of up to 45% for oleyl alcohol and 11% for stearyl alcohol [16]. We also analyzed the kinetics of the reaction using pure methyl oleate and oleic acid [11, 12].

Using oleyl and stearyl acid methyl esters as individual precursors yields valuable oleic and stearic fatty alcohols but the raw materials are expensive. In this sense it is convenient to explore the hydrogenation of alternative fatty feedstocks of lower cost. Biodiesel is a complex mixture of FAMES, with methyl linoleate and methyl oleate being the major components. Methyl linoleate can be hydrogenated to methyl oleate by hydrogenation of the double bond, as a secondary reaction of the system. Unsaturated and saturated fatty alcohols of biodiesel can be selectively hydrogenated to a mixture of fatty alcohols with oleic acid as one of the main products. Stearyl alcohol can also be produced in great yield due to the hydrogenation of stearic acid methyl ester originally present in the mixture, or the saturation of the double bonds of other esters of equal chain length. Then biodiesel can therefore be a convenient raw material for fatty alcohol production. Nowadays the biodiesel market faces some instability due to strict regulations and tariffs that limit access to certain countries, especially the European ones. Consequently, low price unsold biodiesel could be conveniently converted into fatty alcohols of good value and no market restrictions.

Given the complex composition of biodiesel, a selective catalyst is required to hydrogenate the double bonds and carbonyl group, obtaining monounsaturated (oleic alcohol) and saturated (stearyl alcohol) fatty alcohols of commercial value. The overreduction of alcohols to alkanes should be minimal. Supported pure noble metals with high activity for hydrogenolysis of the ester group are also

active for hydrogenation of the alcohol. Tuning the selectivity of the catalyst to restrict secondary undesirable reactions requires modification of the metal function by addition of promoters. Such promotion has been extensively studied for some applications, e.g. the naphtha reforming on Pt and Re catalysts, for which some useful promoters are found to be Sn, Ge, Mg [17–19], that reduce the selectivity to cracking and coking reactions. The same and some other promoters (Sn, Ge, Fe, Cd, B) have been used to modify the activity of noble metals for the transformation of fatty acids and fatty acid methyl esters to fatty alcohols [14], Ru–Sn–B being one of the best combinations found [20].

The aim of this work was to evaluate two ruthenium–tin–boride catalysts, RuSn₂–B/ γ -Al₂O₃ and RuSn₄–B/ γ -Al₂O₃, previously studied for the selective hydrogenation of oleic acid and methyl oleate [15], under different experimental conditions (temperature and pressure) using biodiesel as raw material. Additionally, surface active sites were studied for identifying those participating in the working reaction mechanism. A kinetic model was written using pseudo-components, and rate equations for fatty alcohols production were obtained. Despite of its simplicity this model was able to fit the experimental data very well.

Experimental

Catalyst Preparation

The support used was γ -Al₂O₃ (Cyanamid Ketjen CK-300, pore volume = 0.5 cm³ g⁻¹, S_g (BET) = 180 m² g⁻¹, 35–80 mesh), which underwent calcination for 4 h at 500 °C in an air environment before use. The preparation of the catalyst followed the co-impregnation method described by Shoemaker-Stolk et al. [21]. After impregnation, metal precursors (RuCl₃ and SnCl₂) underwent reduction with a sodium borohydride solution and were left overnight. The catalysts were rinsed repeatedly with distilled water until the solution reached a pH of approximately 7. Finally, activation of the catalysts occurred through hydrogen flow reduction at 300 °C for 2 h. The catalysts were designated as RuSn_x-B, where *x* represents the percentage of Sn (2 and 4 wt%). The percentage of Ru was 1 wt%.

Inductively coupled plasma atomic emission spectroscopy (ICP/OES)

The metallic phase content (Ru, Sn, B) in the catalysts was analyzed using an ICP/OES ARL Model 3410. The composition of the metallic phase was assessed through inductively coupled plasma-optical emission spectroscopy (ICP-OES, PerkinElmer, Optima 2100 DV) following acid digestion and subsequent dilution.

Specific surface area (BET)

The specific surface area of all solids was measured using the BET method [22] at $-196\text{ }^{\circ}\text{C}$ on a Micromeritics ASAP-2000 automatic instrument, covering a range of $0.05 < P/P^0 < 0.27$.

Temperature-programmed reduction (TPR)

Analyses were carried out using equipment equipped with a thermal conductivity detector. The reduction process involved heating from room temperature to $700\text{ }^{\circ}\text{C}$ at a rate of $10\text{ }^{\circ}\text{C min}^{-1}$ in a gaseous stream containing 5.0% H_2 in Ar. Prior to this, the samples underwent calcination at $400\text{ }^{\circ}\text{C}$ for 1 h in an air atmosphere.

Fourier transform infrared absorption spectroscopy (FTIR) of chemisorbed CO

All experiments were conducted within a quartz IR cell fitted with CaF_2 windows, connected to vacuum and atmospheric systems, and situated in a temperature-controlled oven. Prior to analysis, the catalyst was compressed into a self-supported wafer measuring 2 cm^2 (0.5–2 ton) and weighing between 10 and 20 mg. After placing the sample in the IR cell, it underwent overnight reduction at $450\text{ }^{\circ}\text{C}$ in a hydrogen flow (60 mL min^{-1}). Then it was outgassed (10–5 bar) for 2 h and cooled to room temperature. The reference spectrum was captured at room temperature under vacuum (prior to introducing CO into the chamber). All spectra were recorded in the $1000\text{--}4000\text{ cm}^{-1}$ range using a Nicolet 5700 apparatus (resolution: 2 cm^{-1} , 64 analyses per spectrum). Precise volumes of CO were then introduced into the IR cell using a calibrated volume ($V = 0.984\text{ mL}$) until saturation of the sample occurred. After each CO injection, an IR spectrum was recorded, and the spectrum of the adsorbed CO molecules was obtained by subtracting the reference spectra.

X-ray photoelectron spectroscopy (XPS)

XPS measurements were conducted using a SPECS multitechnique apparatus featuring a dual Mg/Al X-ray source and a hemispherical PHOIBOS 150 analyzer operating in the fixed analyzer transmission (FAT) mode. Spectra were acquired with a pass energy of 30 eV, employing an Mg Ka X-ray source at 200 W and 12 kV. The working pressure in the analyzing chamber remained below $5.90 \times 10^{-4}\text{ mPa}$. Solid samples underwent XPS analyses after treatment with hydrogen/argon at $300\text{ }^{\circ}\text{C}$ within the spectrometer's reaction chamber. Spectral regions corresponding to Ru $3d_{5/2}$ and Sn $3d_{5/2}$ core levels were recorded for each sample. Calibration of the spectra utilized the Al $2p$ line (74.4 eV) from an Al_2O_3 support. Casa XPS software (Casa Software Ltd., UK) was employed for data processing. Peak areas were determined through integration after filtering out a Shirley-type background, considering peaks as a combination of Gaussian and Lorentzian functions in a 70/30

ratio. Manufacturer-provided sensitivity factors were used for the quantification of elements.

Transmission electron microscopy (TEM)

The analyses were performed using a JEOL JEM 2100 high-resolution microscope. Sample preparation involved placing the samples in ethanol without prior grinding and subjecting them to an ultrasonic bath. The measurement of particle sizes for histograms was performed using IMAGE.J software. Approximately 200 metal particles were observed for each catalyst, and the distribution of particle sizes was quantified.

Hydrogenation of FAME

The experiments were performed in a stainless steel autoclave reactor with a capacity of 280 cm³. Reaction conditions were adjusted depending on the variable under analysis, while all other parameters remained constant for a duration of 300 min. Each experiment used 1.00 g of catalyst and 20.0 g of distilled soybean biodiesel, sourced from an industry in Santa Fe, Argentina. The study examined the impact of reaction temperatures specifically, at 270 °C, 290 °C, and 320 °C and hydrogen pressure set at 2.04, 4.76, and 6.12 MPa. Reagents and reaction products underwent analysis through GC-FID using a Shimadzu GC-2014 equipped with a Chevron ZB-FFAP capillary column. The analyzes were performed in triplicate to guarantee reproducibility of the results obtained. All reaction products were identified via GC-MS using a Shimadzu QP-5000 instrument featuring an electronic shock source at 260 °C. The instrument was operated with an emission current of 0.70 mA and 70 eV energy. The same GC column employed for the quantitative analysis was used in the GC-MS.

Results and discussion

Characterization of catalysts

The catalysts were characterized by ICP-OES, BET, TPR, FTIR-CO, XPS and TEM [12, 16]. Some of these results were previously published but are presented in this paper to relate the active sites of the catalysts with the activity and performance obtained in the selective hydrogenation of biodiesel.

Table 1 Ru, Sn and B content determined by ICP-OES and specific surface area of the catalysts (BET)

Catalyst	Ru (wt%)	Sn (wt%)	B (wt%)	BET (m ² g ⁻¹)
Ru-B	0.95		0.55	174
RuSn2-B	0.92	1.90	0.38	172
RuSn4-B	0.98	3.65	0.34	171

Table 1 displays the metallic content revealed by ICP-OES, and specific surface area (BET) for the examined catalysts. The measured metal contents were similar to the theoretical values. Additionally, the inclusion of Ru and Sn in the substrate did not affect the specific surface area, $180 \text{ m}^2 \text{ g}^{-1}$, considering the relatively small amount of metal used. The concentration of B exhibited a decreasing trend as the Sn content increased. This was attributed to the greater blocking effect of Sn particles on Ru. This resulted in a reduced amount of reducing agent on the catalyst, indicating that only Ru can undergo reduction.

The temperature-programmed reduction (TPR) traces of both bimetallic and monometallic catalysts are presented in Fig. 1. These results have been previously published [13, 16]. The higher reduction temperature observed for the Sn–B catalysts indicated a more significant interaction between Sn and the support [13]. The monometallic Ru–B/ Al_2O_3 catalysts exhibited a distinct reduction peak at $160 \text{ }^\circ\text{C}$ [13]. In contrast, boron-free monometallic Ru catalysts supported on alumina displayed main reduction peaks at $120 \text{ }^\circ\text{C}$ and $173 \text{ }^\circ\text{C}$, corresponding to the reduction of chlorinated and oxy-chlorinated Ru species, respectively (results not shown) [12, 23]. The shift of these reduction peaks to lower temperatures suggests an enhanced reducibility of the supported metals, indicating an interaction with boron.

The TPR results emphasize the interaction between Ru and Sn in bimetallic catalysts. This interaction is evident through the emergence of co-reduction signals at temperatures distinct from the original peaks observed in monometallic catalysts. The peak at low temperatures, at about $230 \text{ }^\circ\text{C}$ and spanning to $500 \text{ }^\circ\text{C}$,

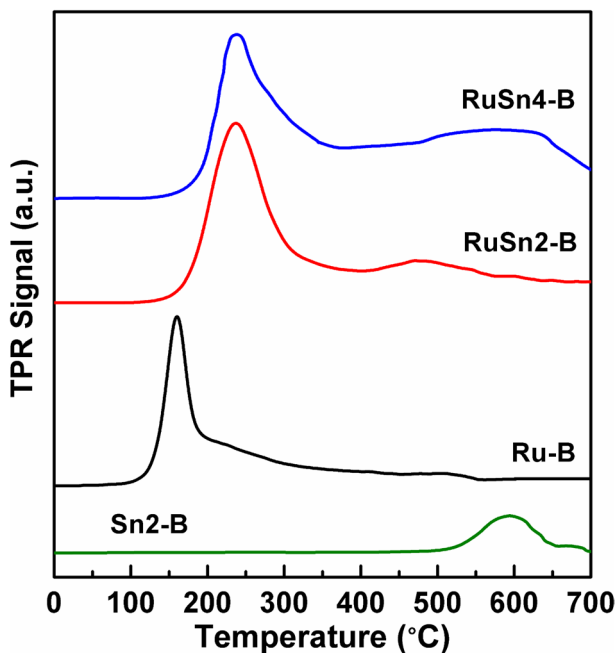
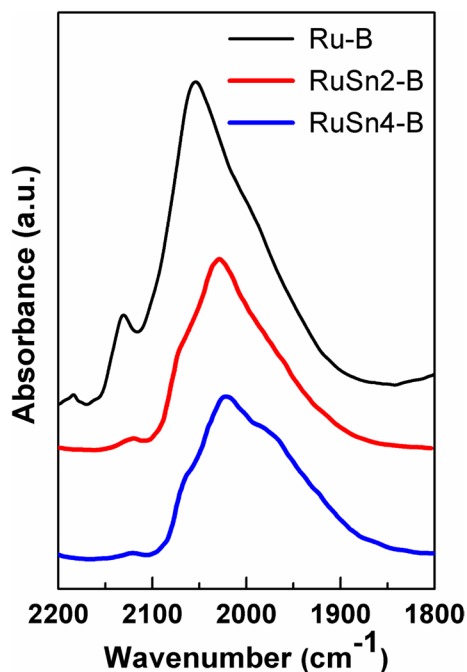


Fig. 1 TPR of monometallic and bimetallic catalyst. From Refs. [13, 16]

Fig. 2 FTIR-CO spectra of monometallic and bimetallic catalysts. From Refs. [12, 16]



could be attributed to a simultaneous reduction of Ru and Sn, while the tail from 200 to 500 °C might be ascribed to Sn species segregated from Ru. Previous research has demonstrated that incorporating sodium borohydride during preparation enhances the interaction between Ru and Sn compared to catalysts prepared through co-impregnation without boron [9].

The FTIR spectra of chemisorbed CO in the 1800–2200 cm⁻¹ wavenumber range are shown in Fig. 2 for the monometallic and bimetallic catalysts. The interaction among the components of the metal function was further studied using FTIR spectroscopy of adsorbed CO. Specifically, CO adsorbs on the Ru metallic sites but not on the Sn sites. CO bands arising from CO adsorption on supported ruthenium catalysts are generally classified into three groups: HF1 (high-frequency 1) at 2156–2133 cm⁻¹, HF2 at 2100–2060 cm⁻¹, and LF (low-frequency) bands at about 2040 ± 40 cm⁻¹ [24]. In the case of the alumina-supported monometallic Ru–B catalysts, the characteristic Ru⁰–CO band at 2052 cm⁻¹ is accompanied by a lower wavelength band around 2133 cm⁻¹, possibly due to the presence of Ru^{δ+} chlorinated species [12, 25]. For bimetallic catalysts, such as RuSn–B/Al₂O₃, it can be observed that the addition of Sn leads to a decrease in the amount of chemisorbed CO, possibly due to a blocking effect on the Ru sites. Conversely, the spectra of the RuSn–B catalyst not only exhibit a reduction in intensity but also significant modifications: the 2133 cm⁻¹ band decreases, and the 2038 cm⁻¹ band shifts to 2025 cm⁻¹, assigned to Ru⁰–CO. These alterations may indicate a substantial modification in the electronic structure of Ru and a reduction in the amount of Ru⁺ species.

Table 2 Ru and Sn surface content determined by XPS

Catalyst	Ru/Al (bulk)	Ru/Al (XPS)	Ru ⁰ / Ru ⁿ⁺ (XPS)	Ru ⁰ /Sn	Sn/Al (bulk)	Sn/Al (XPS)	SnO _x (%)	SnO _y (%)
Ru–B	0.00510	0.0134	0.219	–	–	–	–	–
RuSn2–B	0.00520	0.0100	0.354	13.6	0.00880	0.0196	30.4	69.6
RuSn4–B	0.00530	0.00820	0.800	9.29	0.0181	0.0499	24.0	76.0

Table 2 shows data of the surface atomic ratios obtained from XPS data for the Ru–B, RuSn2–B, and RuSn4–B catalysts. The Ru/Al ratio determined in this way is higher than the apparent ratio obtained through chemical analysis. These results indicate a surface enrichment of Ru in all the catalysts; however, the surface enrichment of Ru (Ru/Al) decreases as the Sn content increases. The fraction of Ru⁰ (Ru⁰/Ruⁿ⁺) increases with the Sn content. Ru is preferentially deposited outside the support particles, likely due to diffusion issues during the impregnation of the Ru salt. A surface enrichment of Ru species on the Al₂O₃ support was previously reported by Pouilloux et al. [26] and Sanchez et al. [16].

It can be observed that the Sn/Al ratios obtained through XPS are higher than the mass-based Sn/Al ratios of the corresponding catalysts. This indicates that in all the catalysts, impregnation leads to a non-uniform distribution of Sn over the support particle. The Ru⁰/Sn ratio is higher in the bimetallic RuSn2–B catalyst. It is interesting to analyze the variation in the fraction of SnO_x and SnO_y with the Sn content. The results from the Table 2 show that the RuSn2-B catalysts have the maximum concentration of SnO_x species (30.4%).

In summary, the XPS results demonstrate that the electronic states of Ru on the catalyst surface depend on the addition of Sn.

Fig. 3a shows characteristic TEM images of the monometallic Ru–B catalyst, illustrating a homogeneous distribution of particles within the 1–4 nm range. Fig. 3b and c demonstrates the TEM images of the bimetallic RuSn–B catalysts. The bimetallic catalyst displays a metal particle distribution focused in the 1–3 nm range, showcasing a reduction in the average particle size due to the addition of Sn.

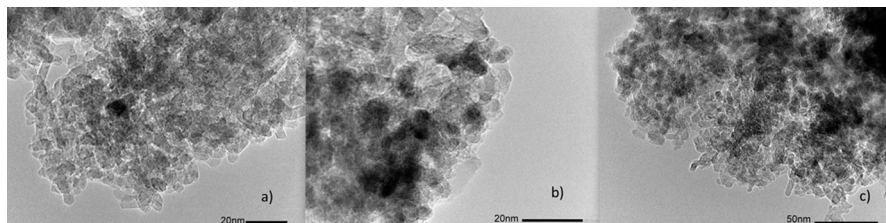
**Fig. 3** TEM images of **a** Ru–B, **b** RuSn2–B, **c** RuSn4–B

Table 3 Mass percentage composition of Soybean biodiesel used as feedstock

Compound	Molecular formula	Composition (wt%)
Methyl palmitate—C16:0	$\text{CH}_3-(\text{CH}_2)_{14}-\text{COOCH}_3$	9.81
Methyl stearate—C18:0	$\text{CH}_3-(\text{CH}_2)_{16}-\text{COOCH}_3$	3.17
Methyl oleate—C18:1	$\text{CH}_3-(\text{CH}_2)_7-\text{CH}=\text{CH}-(\text{CH}_2)_7-\text{COOCH}_3$	26.1
Methyl linoleate—C18:2	$\text{CH}_3-(\text{CH}_2)_4-\text{CH}=\text{CH}-\text{CH}_2-\text{CH}=\text{CH}-(\text{CH}_2)_7-\text{COOCH}_3$	53.6
Methyl linolenate—C18:3	$\text{CH}_3-\text{CH}_2-\text{CH}=\text{CH}-\text{CH}_2-\text{CH}=\text{CH}-\text{CH}_2-\text{CH}=\text{CH}-(\text{CH}_2)_7-\text{COOCH}_3$	7.32

Biodiesel composition

The composition of biodiesel varies depending on the oil feedstock used in its production. In this study, soybean oil was chosen as the preferred biomass-derived oil. The biodiesel was first distilled at reduced pressure to eliminate impurities, including free fatty acids, glycerides, glycerin, and sterols, which might have gone undetected during the analysis. Table 3 presents the mass percentage composition of the distilled biodiesel, determined through gas chromatography analysis. Methyl oleate (C18:1; 26.1%) and methyl linoleate (C18:2; 53.6%) were identified as the main constituents of soybean oil biodiesel, serving as essential precursors for the production of oleyl alcohol. Unlike pure compounds such as methyl oleate and oleic acid used in previous studies for similar determinations, biodiesel is a complex mixture of esters [11–16].

Reaction network

A simplified reaction scheme is shown in Fig. S1 designed to elucidate the hydrogenation results that are explained later. The mechanism describes the hydrogenation of the C=C bond, transforming methyl linolenate (C18:3) into methyl linoleate (C18:2) and subsequently into methyl oleate (C18:1). The direct conversion of methyl oleate leads to the formation of oleyl alcohol [11, 27, 28], oleic acid, and methyl stearate (C18:0). Stearyl alcohol can be subsequently obtained through the hydrogenation of methyl stearate, oleyl alcohol, and stearic acid. Similarly, the reaction of methyl palmitate to palmityl alcohol also occurs [26, 29]. However, due to its low concentration, this palmitate fraction is not included in the overall analysis. Complete hydrogenation of both stearyl and palmityl alcohols results in the formation of paraffinic hydrocarbons (nC16 and nC18). Although other authors have reported the production of heavy esters through transesterification between acids and alcohols, their presence is not presented in the reaction scheme, Fig. S1. [26, 27, 30, 31].

Operative conditions analysis

In the first phase, we assessed chemical control conditions and diffusion limitations for the selective hydrogenation of biodiesel to fatty alcohols. Different stirring speeds were tested and produced consistent results for all reaction products, suggesting the absence of external or internal diffusion control factors.

Hydrogenation of FAME

Firstly, a detailed analysis of the changes occurring in the major esters present in biodiesel should be made. Methyl linolenate has three double bonds (C=C), one of which can be hydrogenated to methyl linoleate. Hydrogenation of the C=O bond can lead to the formation of linolenic alcohol (not detected). Methyl linolenate is not a product of reaction and is only consumed during the reaction. An increase in pressure or temperature leads to a faster disappearance of methyl linolenate. Additionally, the hydrogenation of methyl linolenate is more active with the RuSn2–B catalyst than with the RuSn4–B catalyst (Fig. S2).

In the next step, methyl linoleate can undergo hydrogenation, producing methyl oleate, which is the direct precursor of oleyl alcohol. The linoleic alcohol derived from the hydrogenation of the C=O bond was not detected. The decrease in the molar fraction of methyl linoleate (Fig. S3) occurs at a slower rate than that of methyl linolenate. It can be observed that under more severe reaction conditions (320 °C, 4.76 MPa, and 6.12 MPa), methyl linoleate is rapidly consumed. The hydrogenation of methyl linoleate is more active with the RuSn2–B catalyst than with the RuSn4–B catalyst.

The reactivity of an unsaturated fatty acid should be a result of the position and number of its double bonds: it increases with the number of double bonds and with the distance along the chain [32]. Conjugated C=C double bonds are found to be less reactive when they are closer to the C=O bond [33]. Examining the hydrogenation reaction of a fatty acid with two or three double bonds, such as linoleic acid (C18:2) or linolenic acid (C18:3), it is observed that hydrogen addition occurs in such a way that certain fatty acid radicals are hydrogenated before others. First the linolenic acid is hydrogenated, then the linoleic acid and finally the oleic acid [34], the same can be extrapolated to the esters. The acids are obtained from the direct hydrogenation of the esters. Oleic, stearic, linoleic and palmitic acids were also detected among the reaction products, but in negligible quantities.

Methyl oleate is an intermediate product of the reaction, i.e. is generated and consumed simultaneously, leading to a maximum in its concentration over time, as illustrated in Fig. 4 for the RuSn2–B catalyst and in Fig. S4 for the RuSn4–B catalyst. It can be observed, for both catalysts at 270 °C, a nearly constant concentration of methyl oleate. This is due to an equilibrium between its production and consumption. At higher temperatures and pressures, the peak in the molar fraction shifts to shorter times for both catalysts. A similar trend is observed in the production of methyl stearate, obtained from the hydrogenation of the C=C double bond in methyl

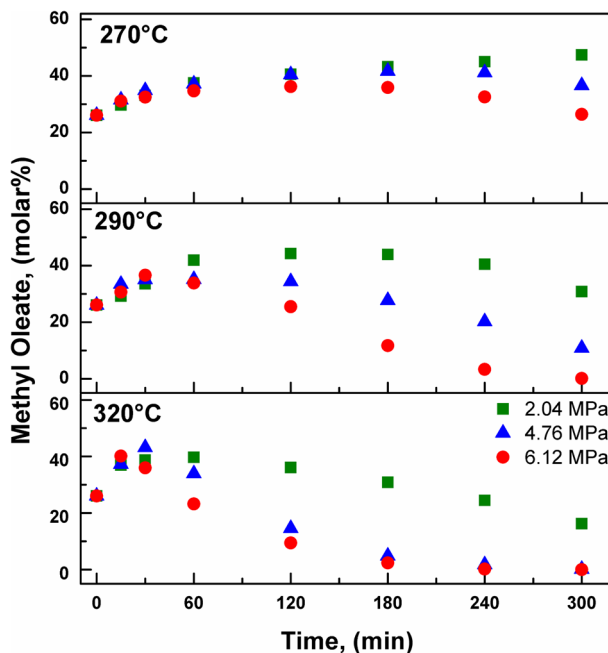


Fig. 4 Molar fraction of methyl oleate as a function of time in the hydrogenation reaction of Biodiesel with the RuSn2-B catalyst. Reaction conditions: Temperature: 270, 290 and 320 °C; Hydrogen Pressure: 2.04, 4.76 and 6.12 MPa; biodiesel mass: 20 g; catalyst mass: 1 g

oleate (results not shown). The main product, oleyl alcohol, is produced through the selective hydrogenation of the carbonyl group $C=O$ in methyl oleate (Fig. S1).

Distribution of products

In this section, the products of the FAME hydrogenation reaction are analyzed, with particular focus on oleyl alcohol due to its significant commercial value. The catalyst and operational conditions that yield the highest oleyl alcohol output will be identified as the most favorable. As seen in the scheme of Fig. S1, oleyl alcohol, methyl stearate and oleic acid are produced through the direct hydrogenation of methyl oleate.

Oleic, stearic, linoleic, and palmitic acids were also detected, but in negligible amounts. All the formed acids reached their maximum before the peak of oleyl alcohol, indicating that acid formation occurred before or along with alcohol formation.

Within the reaction mixture, the combination of fatty acid molecules and fatty alcohols could potentially result in the production of heavy esters through transesterification (undetected product). Pouilloux et al. have suggested that the formation of the heavy ester, oleyl oleate, occurs on tin species without interaction with ruthenium, and the formation rate increases with the content of ruthenium and tin. Oleyl oleate is an intermediate product, and these authors prepared catalysts

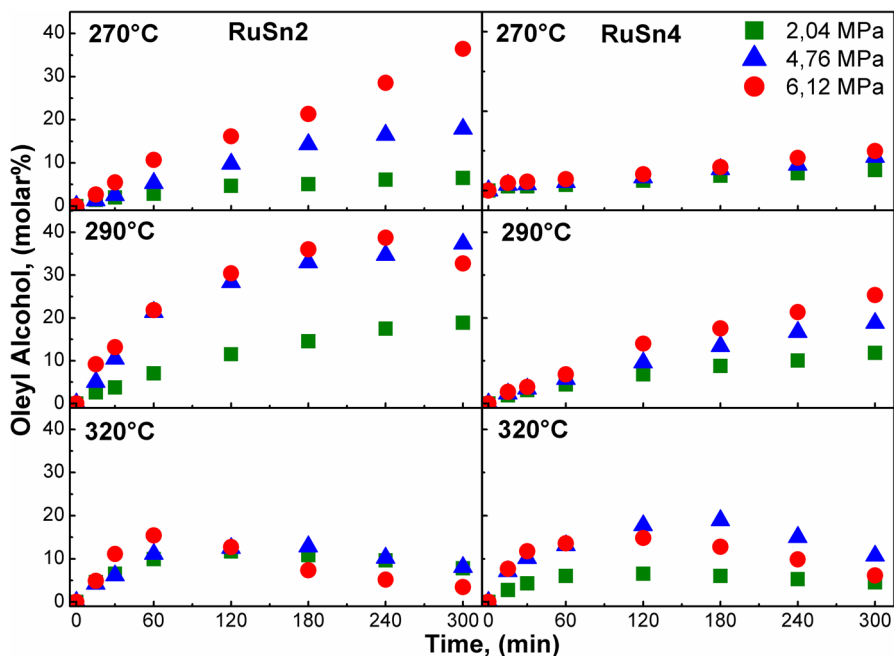


Fig. 5 Molar fraction of Oleyl Alcohol as a function of time in the hydrogenation reaction of Biodiesel. Reaction conditions: Temperature: 270, 290 and 320 °C; hydrogen pressure: 2.04, 4.76 and 6.12 MPa; Biodiesel mass: 20 g; Catalyst mass: 1 g

with 4.1–10 wt% Sn, a much higher content than used in this study. Therefore, it could be inferred that the heavy ester does not form in our case [26].

Fig. 5 represents the molar fraction of oleyl alcohol, a crucial intermediate product, under varying pressure and temperature conditions for two catalysts, RuSn2–B and RuSn4–B. With the RuSn2–B catalyst, oleyl alcohol production reaches a maximum at 290 °C and 6.12 MPa in 240 min. Similar molar fraction values of oleyl alcohol were observed at 290 °C and 4.76 MPa after 300 min of reaction, as well as at 270 °C and 6.12 MPa.

Stearyl alcohol is an intermediate compound resulting from the hydrogenation of methyl stearate, stearic acid, or oleyl alcohol. Consequently, the highest possible stearyl alcohol production is expected to be found at longer reaction times than its precursor compounds. The highest stearyl alcohol production is achieved with the RuSn2–B catalyst. After 240 min of reaction at 290 °C, stearyl alcohol production approached 10% for both pressures, 4.76 and 6.12 MPa. At 320 °C and 6.12 MPa, efficient conversion of stearyl alcohol to octadecane (terminal product) occurred (Fig. S5).

At high pressures and temperatures an increase in the production of octadecane is observed (Fig. S6). Consequently, it is advisable to employ milder conditions to prevent the formation of this undesirable compound and maximize the yield of oleyl alcohol.

Table 4 Percentage of distribution of molar fraction of main products for RuSn2–B

Conditions	Molar fraction (%)				
	Oleyl alcohol	Stearyl alcohol	Alcohols ^a	Octadecane	Alkanes ^b
270 °C 6.12 MPa 300 min	36.4	6.23	45.2	6.03	9.48
290 °C 4.76 MPa 300 min	37.3	11.1	50.3	25.0	29.7
290 °C 6.12 MPa 240 min	38.7	10.2	50.8	34.3	39.5

^a“Alcohols” refers to the combined yield of oleyl, stearic, and palmityl alcohols

^b“Alkanes” correspond to the combined yields of hexadecane and octadecane

In Table 4, the molar fractions of the previously mentioned compounds are listed for RuSn2–B catalysts at the time when the yield of oleyl alcohol is at its peak. It is essential to carefully consider reaction conditions to avoid complete ester hydrogenation present in the biodiesel, which could lead to the formation of alkanes.

At 290 °C, the maximum production of alcohols and alkanes is achieved. In contrast, at 270 °C, a lower production of alkanes is observed for a similar yield of alcohols. Both the operating conditions and the catalyst composition are crucial factors influencing alcohol production.

For the 4% catalyst, a low reactivity toward the double bond is evident, preventing the conversion of methyl oleate to alcohols. The impact on the double bond reaction mechanism in esters due to the addition of Sn can be considered a limiting factor for the alcohol production mechanism to take place.

Reaction mechanisms

To hydrogenate the esters present in biodiesel, it is necessary to hydrogenate both double bonds and the carbonyl group. These two types of bonds exhibit different reactivity. The hydrogenation of the C=C double bond is thermodynamically faster ($\Delta H_{C=C} = -120 \text{ kJ mol}^{-1}$) than the hydrogenation of the C=O carbonyl group ($\Delta H_{C=O} = -50 \text{ kJ mol}^{-1}$) [35–38]. This difference in reactivity appears to be due to the weak polarization of the C=O bond, but also to the steric hindrance characteristic of this functional group [38]. Furthermore, conjugated C=C bonds are less reactive the closer they are to the C=O bond [33].

The differential reactivity of the bonds to be hydrogenated requires that the catalyst have a balanced distribution of active sites to promote the generation of the desired products, the alcohols. In our reaction, the methyl linoleate molecule occupies nearly all available sites on the catalyst surface due to strong multi-site adsorption involving both C=C double bonds and the C=O bond. Deliy et al. demonstrated that the methyl linoleate molecule adsorbs strongly, leading to the formation of two

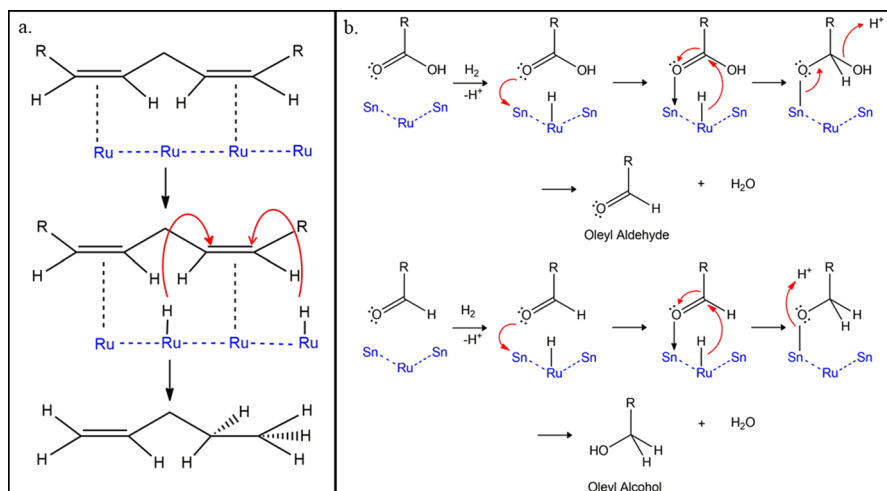


Fig. 6 **a** Mechanism A: hydrogenation of C=C bonds on the RuSn–B catalyst. **b** Mechanism B: hydrogenation of the C=O group on the RuSn–B catalyst

π C=C bonds between the methyl linoleate molecule and the palladium surface atoms [39].

In Fig. 6a, the proposed Mechanism A for the hydrogenation of C=C bonds on the RuSn–B catalyst is depicted. Adsorbed hydrogen occupies all available sites on the catalyst surface. It has been reported that in Ru–Sn supported catalysts, ruthenium is present as Ru^0 in the Ru–Sn system [40]. This site would be involved in the hydrogenation of the C=C bond, which adsorbs onto Ru^0 sites that, along with adjacent Ru–H sites, lead to the formation of methyl oleate from the methyl linoleate molecule. According to the XPS table, the highest Ru⁰/Sn ratio is found in the RuSn2–B catalyst, which aligns with the progression of hydrogenation of double bonds in the precursor compounds. Comparable outcomes were achieved employing monometallic Rh catalysts supported on alumina in the hydrogenation of oleic acid, yielding stearic acid as a reaction product [41]. This suggests that the hydrogenation of the double bond takes place at the Rh^0 sites.

Pouilloux et al. reported that the second proposed site in the RuSn–B catalyst for hydrogenating methyl oleate to oleyl alcohol could be a cluster composed of a Ru atom in close interaction with two oxidized Sn species ($\text{Ru}^0\text{-(SnO}_x)_2$). In accordance with this hypothesis, RuSn2–B shows, by XPS, the highest amount of SnO_x species and the highest selectivity to oleyl alcohol [26]. Fig. 6b presents mechanism B for the hydrogenation of the C=O group. The main effect of tin is to decrease the number of ruthenium atoms on the surface, as observed in the XPS table. Tin activates the C=O group, facilitating hydrogen transfer from adjacent ruthenium sites. The activating effect of tin can be attributed to Sn ions present on the catalytic surface that polarize the carbonyl group. According to FTIR, the addition of Sn decreases the amount of chemisorbed CO, possibly due to a blocking effect of the Ru sites, as also evidenced by XPS. While there is a surface enrichment of Ru^0 with

the addition of Sn, the Ru⁰/Sn ratio decreases, possibly due to a blocking effect on Ru sites. TPR also shows interaction between Ru and Sn, as evidenced by the shift to higher temperatures in the reduction peaks compared to the monometallic catalyst. The RuSn4–B catalyst shows the highest Ru–Sn interaction and segregated Sn. These sites could also explain the increase in ruthenium dispersion with the addition of tin, as evidenced by TEM. This effect is attributed to the spacer effect of SnO between Ru⁰ sites [40].

There is a compromise relationship between these two sites to achieve the highest alcohol production. Site 1 (Ru⁰) generates the necessary precursor (methyl oleate) by hydrogenating the C=C double bond, while at site 2 (Ru⁰–(SnO_x)₂), the carbonyl group is selectively hydrogenated for alcohol production. The RuSn2-B catalyst exhibits an appropriate balance of sites 1 and 2.

Kinetic modeling

To attain a rational interpretation of the results, a kinetic model was proposed for the catalyst with the best performance for the formation of oleyl alcohol from FAME, i.e. the RuSn2–B catalyst. In a previous study a comprehensive analysis of all possible mechanisms was done for the case of the hydrogenation of oleic acid to oleyl alcohol [42]. A big number of reaction mechanisms were proposed and assessed. The best mechanism was the one with the following hypotheses: (i) only one type of adsorption site is required for all species and reactions; (ii) H₂ is dissociatively adsorbed; (iii) fatty molecules are adsorbed on only one site; (iv) pairwise insertion of H onto fatty molecules is the rate-limiting step; (v) reduction of the carboxylate group occurs via an aldehyde intermediate which is subsequently hydrogenated to the corresponding alcohol; (vi) hydrogen and oleic acid are the major adsorbates; (vii) wax heavy esters are formed but do not contribute as intermediates to the main mechanism. It was also reported from the Gibbs free energy analysis that the reactions were irreversible at the reaction conditions of that work [42]. This also applies to the conditions of this work.

Mathematical procedure

Ad-hoc developed programs and software tools from the Octave package for Windows were used for the treatment of the kinetic data. A procedure described in a previous report was used [42, 43]. The implemented optimization procedure minimized the sum of the squares (χ^2) of the deviations between the actual (experimental) and predicted (model) concentration values. From the comparison of the values of χ^2 , the discrimination between models was made. Calculation of (χ^2) was made using all runs and all the considered compounds, as indicated in Eq. 1. m is the index of the detectable compounds ($m = 1, \dots, 15$) and j is the index of the experimental run ($j = 1, \dots, 9$). This means that reactants and products entering the summation of the error χ^2 are only those that can be identified and measured.

$$\chi^2 = \sum_{runs,j=1}^9 \left[\sum_{compounds,m=1}^{15} \left(C_{m,j}^{exp} - C_{m,j}^{theo} \right)^2 \right] \quad (1)$$

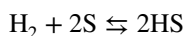
$$\min (\chi^2 + \Theta) \quad (2)$$

$$\Theta = [10^6 \text{ for } p_k < 0; 0 \text{ for } p_k \geq 0, \quad \forall k] \quad (3)$$

Minimization was performed using the Simplex algorithm of Nelder and Mead [44], as implemented in Octave for Windows, that uses a modification introduced by Lagarias et al. [43]. This algorithm is one for unconstrained problems. Restrictions were thus considered by introducing a penalty function Θ (Eq. 2). The penalty used was just a sufficiently big step term added when the restrictions were violated (Eq. 3). k is the index of the adjustable parameters of the optimization procedure.

Mechanism

To express the dissociative adsorption of hydrogen on the S sites, the following equation was used [45]:

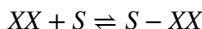


The equation corresponding to the mass action law of thermodynamic equilibrium for the previous reaction can be written as:

$$K_{\text{H}_2}^{ads} = \frac{C_{SH}^2}{C_S^2 \cdot P_{\text{H}_2}} \quad (4)$$

C_{SH} is the concentration of adsorbed hydrogen atoms on the active sites. C_S is the concentration of active sites that are free for adsorption and P_{H_2} is the partial pressure of hydrogen in the gas phase. Since the reaction occurs with molecular hydrogen dissolved in the liquid phase, the equilibrium constant in this equation is really a combination of the real thermodynamic constant for hydrogen adsorption, the Henry's constant accounting for the solubility of H_2 in the liquid phase, and the activity coefficients accounting for the non-idealities of the liquid and gas phase.

The adsorption of the organic molecules can be written as:



The equilibrium action mass law for this reaction can be written as in Eq. 5. C_{XX} is the concentration of the organic compounds in the liquid phase.

$$K_{XX}^{ads} = \frac{C_{S-XX}}{C_S \cdot C_{XX}} \quad (5)$$

Considering the adsorption of the ester and acid compounds, the total site balance is:

$$C_T = C_S + C_{HS} + C_{S-acids} + C_{S-esters} + C_{S-alcohols} \quad (6)$$

In this equation, C_T is the total concentration of active sites of the catalysts, C_S is the concentration of free adsorption sites, C_{HS} is the concentration of surface adsorbed hydrogen, C_{S-acid} is the concentration of the surface adsorbed acids, C_{S-ols} is concentration of surface adsorbed alcohols and $C_{S-esters}$ is concentration of surface adsorbed esters. The free concentration of sites was calculated using Eq. 7.

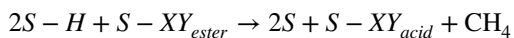
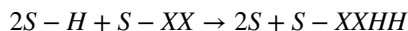
$$C_S = \frac{C_T}{\left[1 + \sqrt{P_{H_2} \cdot K_{H_2}^{ads}} + K^{ads} \cdot (C_{acids} + C_{alcohols} + C_{esters})\right]} = \frac{C_T}{ADS} \quad (7)$$

Some assumptions are evident in the previous equations. (i) No individual compounds are distinguished and lumps of acids, alcohols and esters, are used instead. In this sense, no distinctions are made between oleic, linoleic and linolenic esters, indicating that reactivity and adsorption are supposed to be dominated by the chemistry of the group rather than secondary features such as molecular size or number of double bonds. The same applies to acids and alcohols. (ii) All organic molecules are supposed to have similar adsorption constants. This was really a result of the data fitting procedure, that indicated that considering different constants for each reactant did not yield much better results. (iii) Alkanes (octadecane and hexadecane), products of hydrode-oxygenation of the alcohols, are considered to adsorb in negligible amounts and are not included in the summation of adsorbates.

Replacing Eq. 7 in the adsorption of each organic molecule (Eq. 5):

$$C_{S-XX} = K_{XX} \cdot \frac{C_T}{ADS} \cdot C_{XX} \quad (8)$$

The two hydrogenation reactions of the system are double bond C=C hydrogenation of unsaturated XX compounds and hydrogenation of XY methyl esters to XY acids and methanol (see below).



Assuming that catalyst deactivation is negligible and that the reaction orders are all unitary, the rates of reaction of these two kinds of hydrogenation can be written in a common generic form (Eq. 9) or a detailed one (Eqs. 10–11). In these equations, C_{XX} and C_{XY} are the concentration of unsaturated compounds and fatty acid methyl esters, respectively.

$$r_i = k_i \cdot C_{S-H}^2 \cdot C_{S-XX} \quad (9)$$

$$r_i = \frac{k_i \cdot K_{H_2}^{ads} \cdot K_{XXester}^{ads}}{ADS^3} \cdot P_{H_2} \cdot C_{XXester} \quad (10)$$

Table 5 Expression of the reaction rate for the individual compounds

Reaction	Reactive	Product	Reaction rate
1	LLM+H ₂	LM	$r_1 = \frac{k_1 \cdot K_{H_2}^{ads} K_{LLM}^{ads}}{ADS^3} \cdot P_{H_2} \cdot C_{LLM}$
2	LM+H ₂	OM	$r_2 = \frac{k_2 \cdot K_{H_2}^{ads} K_{LM}^{ads}}{ADS^3} \cdot P_{H_2} \cdot C_{LM}$
3	OM+H ₂	AO+CH ₄	$r_3 = \frac{k_3 \cdot K_{H_2}^{ads} K_{OM}^{ads}}{ADS^3} \cdot P_{H_2} \cdot C_{OM}$
4	LM+H ₂	AL+CH ₄	$r_4 = \frac{k_4 \cdot K_{H_2}^{ads} K_{LM}^{ads}}{ADS^3} \cdot P_{H_2} \cdot C_{LM}$
5	OM+H ₂	EM	$r_5 = \frac{k_5 \cdot K_{H_2}^{ads} K_{OM}^{ads}}{ADS^3} \cdot P_{H_2} \cdot C_{OM}$
6	AL+H ₂	AO	$r_6 = \frac{k_6 \cdot K_{H_2}^{ads} K_{AL}^{ads}}{ADS^3} \cdot P_{H_2} \cdot C_{AL}$
7	AO+2 H ₂	ALO+H ₂ O	$r_7 = \frac{k_8 \cdot K_{H_2}^{ads2} \cdot K_{AO}^{ads}}{ADS^5} \cdot P_{H_2}^2 \cdot C_{AO}$
8	AO+H ₂	AE	$r_8 = \frac{k_{10} \cdot K_{H_2}^{ads} K_{AO}^{ads}}{ADS^3} \cdot P_{H_2} \cdot C_{AO}$
9	ALO+H ₂	ALE	$r_9 = \frac{k_{11} \cdot K_{H_2}^{ads} K_{ALO}^{ads}}{ADS^3} \cdot P_{H_2} \cdot C_{ALO}$
10	EM+H ₂	AE+CH ₄	$r_{10} = \frac{k_{12} \cdot K_{H_2}^{ads} K_{EM}^{ads}}{ADS^3} \cdot P_{H_2} \cdot C_{EM}$
11	AE+2H ₂	ALE+H ₂ O	$r_{11} = \frac{k_{13} \cdot K_{H_2}^{ads2} \cdot K_{AE}^{ads}}{ADS^5} \cdot P_{H_2}^2 \cdot C_{AE}$
12	ALE+H ₂	C ₁₈ +H ₂ O	$r_{12} = \frac{k_{14} \cdot K_{H_2}^{ads} K_{ALE}^{ads}}{ADS^3} \cdot P_{H_2} \cdot C_{ALE}$
13	PM+H ₂	ALP+CH ₄	$r_{13} = \frac{k_{15} \cdot K_{H_2}^{ads} K_{PM}^{ads}}{ADS^3} \cdot P_{H_2} \cdot C_{PM}$
14	AP+2 H ₂	ALP+H ₂ O	$r_{14} = \frac{k_{16} \cdot K_{H_2}^{ads2} \cdot K_{AP}^{ads}}{ADS^5} \cdot P_{H_2}^2 \cdot C_{AP}$
15	ALP+H ₂	C ₁₆ +H ₂ O	$r_{15} = \frac{k_{17} \cdot K_{H_2}^{ads} K_{ALP}^{ads}}{ADS^3} \cdot P_{H_2} \cdot C_{ALP}$
16	OM+2 H ₂	ALO+CH ₃ OH	$r_{16} = \frac{k_7 \cdot K_{H_2}^{ads2} \cdot K_{OM}^{ads}}{ADS^5} \cdot P_{H_2}^2 \cdot C_{OM}$
17	EM+2 H ₂	ALE+CH ₃ OH	$r_{17} = \frac{k_9 \cdot K_{H_2}^{ads2} \cdot K_{EM}^{ads}}{ADS^5} \cdot P_{H_2}^2 \cdot C_{EM}$
18	PM+2 H ₂	ALP+CH ₃ OH	$r_{18} = \frac{k_{18} \cdot K_{H_2}^{ads2} \cdot K_{PM}^{ads}}{ADS^5} \cdot P_{H_2}^2 \cdot C_{PM}$

PM, EM, LLM, LM, OM: palmitic, stearic, linolenic, linoleic and oleic methyl esters

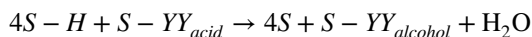
AP, AE, ALL, AL, AO: palmitic, stearic, linolenic, linoleic and oleic fatty acids

C₁₆, C₁₈: hexadecane, octadecane

ALO, ALE, ALP: oleic, stearic and palmitic fatty alcohols

$$r_i = \frac{k_i \cdot K_{H_2}^{ads} \cdot K_{XYacid}^{ads}}{ADS^3} \cdot P_{H_2} \cdot C_{XYacid} \quad (11)$$

Finally, the reaction of hydrogenation of the fatty acids YY_{acid} to fatty alcohols $YY_{alcohol}$ must be considered (see below) and its reaction rate written (Eq. 12)



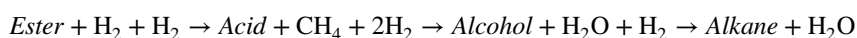
$$r_i = \frac{k_i \cdot K_{H_2}^{ads2} \cdot K_{YYacid}^{ads}}{ADS^5} \cdot P_{H_2}^2 \cdot C_{YYacid} \quad (12)$$

k_i would be the kinetic constant of reaction i . Considering each chemical reaction separately, all developed rate equations are shown in Table 5. These rate expressions have been derived using the Hougen-Watson formalism, in which one elementary step of the mechanism is considered to be rate-limiting, and the other steps are considered to be in equilibrium.

Equations for the production of fatty alcohols from highly unsaturated methyl esters are not written since from the results it can be inferred that linoleic and linolenic methyl esters are first rapidly hydrogenated to oleic and stearic methyl esters. The reaction mechanism thus laid out leads to a mathematical model with several parameters. In fact, 18 kinetic reaction constants and 4 adsorption constants.

As explained before no distinction can be made between individual organic compounds concerning adsorption, with regards to its kind of terminal group (acid, ester, alcohol) or the degree of insaturation. Hence the set of adsorption constants can be reduced to only one. Also a constant for adsorption of hydrogen had to be considered.

If the kinetic constants are grouped in attention to the kind of reaction irrespective of the starting molecule, the number of kinetics constants can be reduced to three, and the reactants can be grouped in a set represented by a pseudocompound (ester, acid, alcohol, alkane). The *Alkane* pseudocompound represents the alkane mixture $C_{16} + C_{18}$. Then the reaction mechanism could now be written in terms of the pseudocompounds:



Considering that all the compounds are adsorbed on the catalyst, the following equations can be determined:

$$\text{Ester to acid} \quad r_1 = \frac{k_1}{ADS^3} \cdot P_{H_2} \cdot C_{ester}$$

$$\text{Acid to alcohol} \quad r_2 = \frac{k_2}{ADS^5} \cdot P_{H_2}^2 \cdot C_{acid}$$

$$\text{Alcohol to alkane} \quad r_3 = \frac{k_3}{ADS^3} \cdot P_{H_2} \cdot C_{alcohol}$$

$$ADS = \left[1 + \sqrt{P_{H_2} \cdot K_{H_2}^{ads}} + K^{ads} \cdot (C_{acid} + C_{ols} + C_{Esters}) \right]$$

This model has only 5 parameters to be determined: two adsorption constants ($K_{H_2}^{ads}$ and K^{ads}) and three kinetic constants (k_1, k_2, k_3). Theoretical values were obtained by using experimental concentration values from 9 experiences. Each run was carry out with a different combination of hydrogen pressure and

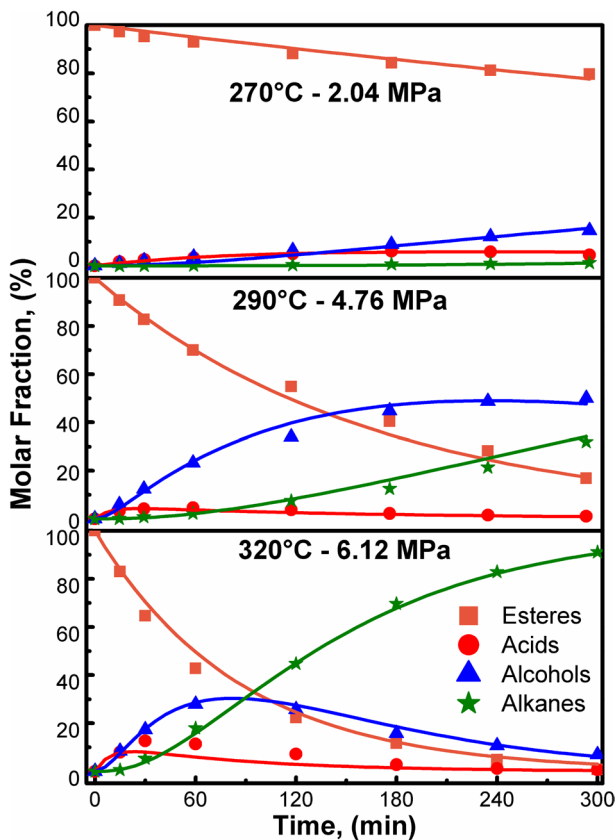


Fig. 7 Comparison between experimental values (points) and theoretically predicted values (solid lines). RuSn2–B catalyst. Reaction conditions: temperature: 270, 290 and 320 °C; hydrogen pressure: 2.04, 4.76 and 6.12 MPa; biodiesel mass: 20 g; catalyst mass: 1 g

temperature. Kinetic and adsorption constants were adjusted for each temperature separately using the mathematical procedure described above. Dependence of parameters with temperature was analyzed by Arrhenius equation for kinetic constants and Van't Hoff equation for adsorption constants.

Fig. 7 displays the comparison between experimental and theoretical values obtained using the simple model of five parameters. The graph depicts the total concentration of alkanes, esters, alcohols, and acids over reaction time for the RuSn2–B catalyst under the studied pressure and temperature conditions, presenting both experimental and theoretical results. From the graph, it can be concluded that the simple pseudo-compound model offers a satisfactory fit to the experimental data. The diagram presents a comparison of the experimental results (points) and the prediction of the proposed model (solid line).

Conclusions

This study demonstrated that the most active and selective catalyst for the formation of oleyl alcohol through the hydrogenation of FAME was RuSn₂-B. When using the RuSn₂-B catalyst, oleyl alcohol production peaks at 290 °C and 6.12 MPa after 240 min. Similar molar fraction values of oleyl alcohol were observed at 290 °C and 4.76 MPa after 300 min of reaction, as well as at 270 °C and 6.12 MPa. It is observed that at 290 °C, the maximum production of alcohols and alkanes is achieved. In contrast, at 270 °C, a lower production of alkanes is observed for a similar yield of alcohols. At 290 °C, the pressure effect does not have a significant impact, so it is advisable to use the lowest possible hydrogen pressure to reduce costs associated with compression and recirculation. Both operational conditions and catalyst composition are crucial factors influencing alcohol production.

According to the results obtained from the biodiesel hydrogenation and the characterization analysis of the catalysts, two types of sites were identified: Site 1 (Ru⁰), which generates the necessary precursor (methyl oleate) by hydrogenating the C=C double bond, and Site 2 (Ru⁰-(SnO_x)₂), where the carbonyl group is selectively hydrogenated for alcohol production. There is a compromise relationship between these two sites to achieve the highest alcohol production. The RuSn₂-B catalyst exhibits an appropriate balance of sites 1 and 2.

An analysis was conducted on the experimental reaction data using a simple kinetic model. The model takes into account the reactions of esters to fatty acids, fatty acids to alcohols, and alcohols to deoxygenated hydrocarbons. The results indicate that the simple model, utilizing pseudo-compounds, provides a reliable fit of the experimental data.

Supplementary Information The online version contains supplementary material available at <https://doi.org/10.1007/s11144-024-02661-7>.

Acknowledgements The authors thank CONICET (PIP 2021-2023 Grant 11220200100786CO) and UNL (CAI+D-2020 Grants 50620190100073LI) for the financial support of this work.

Data availability Supporting data is available from the authors upon request. The corresponding author should be contacted for this.

References

1. Hill K (2000) Fats and oils as oleochemical raw materials. *Pure Appl Chem* 72:1255–1264. <https://doi.org/10.1351/pac200072071255>
2. Turek T, Trimm DL, Cant NW (1994) The catalytic hydrogenolysis of esters to alcohols. *Catal Rev* 36:645–683. <https://doi.org/10.1080/01614949408013931>
3. Fortune Business Insight Homepage <https://www.fortunebusinessinsights.com>
4. Rupilius W, Ahmad S (2007) Palm oil and palm kernel oil as raw materials for basic oleochemicals and biodiesel. *Eur J Lipid Sci Technol* 109:433–439. <https://doi.org/10.1002/ejlt.200600291>
5. Haupt DE, Drinkard G, Pierce HF (1984) Future of petrochemical raw materials in oleochemical markets. *J Am Chem Soc* 61:276–281. <https://doi.org/10.1007/BF02678781>
6. Thakur DS, Kundu A (2016) Catalysts for fatty alcohol production from renewable resources. *J Am Oil Chem Soc* 93:1575–1593. <https://doi.org/10.1007/s11746-016-2902-x>

7. Pouilloux Y, Autin F, Barrault J (2000) Selective hydrogenation of methyl oleate into unsaturated alcohols: relationships between catalytic properties and composition of cobalt–tin catalysts. *Catal Today* 63:87–100. [https://doi.org/10.1016/S0920-5861\(00\)00448-X](https://doi.org/10.1016/S0920-5861(00)00448-X)
8. Narasimhan CS, Deshpande VM, Ramnarayan K (1989) Selective hydrogenation of methyl oleate to oleyl alcohol on mixed ruthenium–tin boride catalysts. *Appl Catal* 48:L1–L6. [https://doi.org/10.1016/S0166-9834\(00\)80260-2](https://doi.org/10.1016/S0166-9834(00)80260-2)
9. Sánchez MA, Mazzieri VA, Sad MR, Grau R, Pieck CL (2011) Influence of preparation method and boron addition on the metal function properties of Ru–Sn catalysts for selective carbonyl hydrogenation. *J Chem Technol Biotechnol* 86:447–453. <https://doi.org/10.1002/jctb.2536>
10. Rodina VO, Ermakov DY, Saraev AA, Reshetnikov SI, Yakovlev VA (2017) Influence of reaction conditions and kinetic analysis of the selective hydrogenation of oleic acid toward fatty alcohols on Ru–Sn–B/Al₂O₃ in the flow reactor. *Appl Catal B* 209:611–620. <https://doi.org/10.1016/j.apcatb.2017.03.012>
11. Sánchez MA, Mazzieri VA, Sad MR, Pieck CL (2012) Influence of the operating conditions and kinetic analysis of the selective hydrogenation of methyl oleate on Ru–Sn–B/Al₂O₃ catalysts. *Reac Kinet Mech Cat* 107:127–139. <https://doi.org/10.1007/s11144-012-0465-x>
12. Sánchez MA, Pouilloux Y, Mazzieri VA, Pieck CL (2013) Influence of the operating conditions and kinetic analysis of the selective hydrogenation of oleic acid on Ru–Sn–B/Al₂O₃ catalysts. *Appl Catal A* 467:552–558. <https://doi.org/10.1016/j.apcata.2013.08.014>
13. Sánchez MA, Mazzieri VA, Vicerich MA, Vera CR, Pieck CL (2015) Deactivation study of Ru–Sn–B/Al₂O₃ catalysts during selective hydrogenation of methyl oleate to fatty alcohol. *Ind Eng Chem Res* 54:6845–6854. <https://doi.org/10.1002/ce.23444>
14. Sánchez MA, Torres GC, Mazzieri VA, Pieck CL (2017) Selective hydrogenation of fatty acids and methyl esters of fatty acids to obtain fatty alcohols—a review. *J Chem Technol Biotechnol* 92:27–42. <https://doi.org/10.1002/jctb.5039>
15. Sánchez MA, Mazzieri VA, Pronier S, Vicerich MA, Especel C, Epron F, Pieck CL (2019) Ru–Sn–B/TiO₂ catalysts for methyl oleate selective hydrogenation. influence of the preparation method and the chlorine content. *J Chem Technol Biotechnol* 94:982–991. <https://doi.org/10.1002/jctb.5849>
16. Sánchez MA, Mazzieri VA, Vicerich MA, Vera CR, Pieck CL (2015) Ru–Sn–B/Al₂O₃ catalysts for selective hydrogenation of methyl oleate: influence of the Ru/Sn ratio. *J Chem* 561350:7. <https://doi.org/10.1155/2015/561350>
17. D’Ippolito SA, Vera CR, Epron F, Samoila P, Especel C, Marecot P, Gutierrez LB, Pieck CL (2009) Influence of tin addition by redox reaction in different media on the catalytic properties of Pt–Re/Al₂O₃ naphtha reforming catalysts. *Appl Catal A* 370:34–41. <https://doi.org/10.1016/j.apcata.2009.09.012>
18. D’Ippolito SA, Vera CR, Epron F, Especel C, Marécot P, Pieck CL (2007) Naphtha reforming Pt–Re–Ge/γ-Al₂O₃ catalysts prepared by catalytic reduction: influence of the pH of the Ge addition step. *Catal Today* 133:13–19. <https://doi.org/10.1016/j.cattod.2007.11.014>
19. D’Ippolito SA, Gutierrez LB, Vera CR, Pieck CL (2012) Pt–Mg–Ir/Al₂O₃ and Pt–Ir/HY zeolite catalysts for SRO of decalin. Influence of Ir content and support acidity. *Appl Catal A* 452:48–56. <https://doi.org/10.1016/j.apcata.2012.12.002>
20. Deshpande VM, Ramnarayan K, Narasimhan CS (1990) Studies on ruthenium–tin boride catalysts II. Hydrogenation of fatty acid esters to fatty alcohols. *J Catal* 121:174–182. [https://doi.org/10.1016/0021-9517\(90\)90227-B](https://doi.org/10.1016/0021-9517(90)90227-B)
21. Schoenmaker-Stolk MC, Verwijs JW, Scholten JJF (1987) The catalytic hydrogenation of benzene over supported metal catalysts. III. Gas-phase hydrogenation of benzene over silica-supported Ru–Cu catalysts. *Appl Catal* 30:339–352. [https://doi.org/10.1016/S0166-9834\(00\)84124-X](https://doi.org/10.1016/S0166-9834(00)84124-X)
22. Brunauer S, Emmett PH, Teller E (1938) Adsorption of gases in multimolecular layers. *J Am Chem Soc* 60:309–319. <https://doi.org/10.1021/ja01269a023>
23. Bossi A, Garbassi F, Orlandi A, Petrini G (1979) Preparation aspects of Ru-supported catalysts and their influence on the final products. *Stud Surf Sci Catal* 3:405–416. [https://doi.org/10.1016/S0167-2991\(09\)60227-5](https://doi.org/10.1016/S0167-2991(09)60227-5)
24. Hadjiivanov K, Lavalley JC, Lamotte J, Maugé F, Saint-Just J, Chez M (1998) FTIR study of CO interaction with Ru/TiO₂ catalysts. *J Catal* 176:415–425. <https://doi.org/10.1006/jcat.1998.2038>
25. Narita T, Miura H, Sugiyama K, Matsuda T, Gonzalez RD (1987) The effect of reduction temperature on the chemisorptive properties of RuSiO₂: effect of chlorine. *J Catal* 103:492–495. [https://doi.org/10.1016/0021-9517\(87\)90140-0](https://doi.org/10.1016/0021-9517(87)90140-0)
26. Pouilloux Y, Autin F, Guimon C, Barrault J (1998) Hydrogenation of fatty esters over ruthenium–tin catalysts; characterization and identification of active centers. *J Catal* 176:215–224. <https://doi.org/10.1006/jcat.1998.2044>

27. Echeverri DA, Marín JM, Restrepo GM, Rios LA (2009) Characterization and carbonylic hydrogenation of methyl oleate over Ru–Sn/Al₂O₃: effects of metal precursor and chlorine removal. *Appl Catal A* 366:342–347. <https://doi.org/10.1016/j.apcata.2009.07.029>
28. Ishii K, Mizukami F, Niwa S, Toba M, Ushijima H, Sato T (1996) Effects of raw materials and preparation methods of catalysts on the selective hydrogenation of ethyl phenylacetate. *J Am Oil Chem Soc* 73:465–469. <https://doi.org/10.1007/BF02523920>
29. Miyake T, Makino T, Taniguchi S, Watanuki H, Niki T, Shimizu S, Kojima Y, Sano M (2009) Alcohol synthesis by hydrogenation of fatty acid methyl esters on supported Ru–Sn and Rh–Cn catalysts. *Appl Catal A* 364:108–112. <https://doi.org/10.1016/j.apcata.2009.05.036>
30. Sagata K, Hirose M, Hirano Y, Kita Y (2016) Transformation of methyl laurate into lauryl alcohol over a Ru–Sn–Mo/C catalyst by using zerovalent iron and water as an in situ hydrogen source. *Appl Catal A* 523:85–91. <https://doi.org/10.1016/j.apcata.2016.05.022>
31. Taniguchi SI, Makino T, Watanuki H, Kojima YU, Sano M, Miyake T (2011) Effect of Pt addition to Ru–Sn/Al₂O₃ catalyst on hydrogenation of methyl laurate. *Appl Catal A* 397:171–173. <https://doi.org/10.1016/j.apcata.2011.02.024>
32. Morrison RT, Boyd RN (1998) *Química orgánica*, 5ª. Addison Wesley, México
33. Kluson P, Cervený L (1994) Preparation and properties of ruthenium supported catalysts. *Catal Lett* 23:299–312. <https://doi.org/10.1007/BF00811365>
34. Veldsink JW, Bouma MJ, Schoon NH, Beenackers AACM (1997) Heterogeneous hydrogenation of vegetable oils: a literature review. *Catal Rev Sci Eng* 39:253–318. <https://doi.org/10.1080/01614949709353778>
35. Richter JD (1968) High pressure hydrogenation of unsaturated fatty acids to unsaturated fatty alcohols, Thesis Technische Universiteit Delft, ed. Delft, Verenigde drukkerrijen Judels, Brinkma.
36. Ponce V (1997) On the role of promoters in hydrogenations on metals; α - β unsaturated aldehydes and ketones. *Appl Catal A* 149:27–48. [https://doi.org/10.1016/S0926-860X\(96\)00250-5](https://doi.org/10.1016/S0926-860X(96)00250-5)
37. Ekou T, Vicente A, Lafaye G, Especel C, Marecot P (2006) Bimetallic Rh–Ge and Pt–Ge catalysts supported on TiO₂ for citral hydrogenation: I. Preparation and characterization of the catalysts. *Appl Catal A* 314:64–72. <https://doi.org/10.1016/j.apcata.2006.08.003>
38. Castro-Grijalba A, Urresta J, Ramirez A, Barrault J, Argent J (2011) Preparation and characterization of catalysts based on cassiterite (SnO₂) and its application in hydrogenation of methyl esters. *Chem Soc* 98:48–59. <https://doi.org/10.25100/rc.v17i3.481>
39. Deliy IV, Maksimchuk NV, Psaro R, Ravasio N, Dal Santo V, Recchia S, Paukshtis EA, Golovin AV, Semikolenov VA (2005) Kinetic peculiarities of *Cis/trans* methyl oleate formation during hydrogenation of methyl linoleate over Pd/MgO. *Appl Catal A* 279:99–107. <https://doi.org/10.1016/j.apcata.2004.10.017>
40. Desphande VM, Patterson WR, Narashimahn CS (1990) Studies on ruthenium-tin boride catalysts. I. Characterization. *J Catal* 121:165–173. [https://doi.org/10.1016/0021-9517\(90\)90226-A](https://doi.org/10.1016/0021-9517(90)90226-A)
41. Fonseca Benítez CA, Mazzieri VA, Sánchez MA, Benítez VM, Pieck CL (2019) Selective hydrogenation of oleic acid to fatty alcohols on Rh–Sn–B/Al₂O₃ catalysts. Influence of Sn content. *Appl Catal A* 584:117149–117156. <https://doi.org/10.1016/j.apcata.2019.117149>
42. Fonseca Benítez CA, Mazzieri VA, Vera CR, Benítez VM, Pieck CL (2021) Selective hydrogenation of oleic acid to fatty alcohols over a Rh–Sn–B/Al₂O₃ catalyst: kinetics and optimal reaction conditions. *React Chem Eng* 6:726–746. <https://doi.org/10.1039/D0RE00488J>
43. Lagarias JC, Reeds JA, Wright MH, Wright PE (1998) Convergence properties of the Nelder–Mead simplex algorithm in low dimensions. *SIAM J Optim* 9:112–147. <https://doi.org/10.1137/S1052623496303470>
44. Nelder JA, Mead R (1965) A simplex method for function minimization. *Comput J* 7(4):308–313. <https://doi.org/10.1093/comjnl/7.4.308>
45. Efremenko I (2001) Implication of palladium geometric and electronic structures to hydrogen activation on bulk surfaces and clusters. *J Mol Catal A* 173:19–59. [https://doi.org/10.1016/S1381-1169\(01\)00144-3](https://doi.org/10.1016/S1381-1169(01)00144-3)

Publisher's Note Springer Nature remains neutral with regard to jurisdictional claims in published maps and institutional affiliations.

Springer Nature or its licensor (e.g. a society or other partner) holds exclusive rights to this article under a publishing agreement with the author(s) or other rightsholder(s); author self-archiving of the accepted manuscript version of this article is solely governed by the terms of such publishing agreement and applicable law.